Mapping Neurogenesis Onset in the Optic Tectum of Xenopus Laevis

Research Article

Developmental Neurobiology
DOI 10.1002/dneu.22393

Mapping neurogenesis onset in the optic tectum of *Xenopus laevis*

Leah Herrgen[1-3] and Colin J. Akerman[1,*]

[1]Department of Pharmacology, University of Oxford, Mansfield Road, Oxford OX1 3QT, UK. [2]Centre for Neuroregeneration, University of Edinburgh, 49 Little France Crescent, Edinburgh EH16 4SB, UK. [3]Euan MacDonald Centre for Motor Neurone Disease Research, University of Edinburgh, Edinburgh EH16 4SB, UK

*Author for correspondence (colin.akerman@pharm.ox.ac.uk)

Short title

Mapping neurogenesis onset in *Xenopus*

Received: Dec 24, 2015; Revised: Mar 22, 2016; Accepted: Mar 22, 2016

ABSTRACT

Neural progenitor cells have a central role in the development and evolution of the vertebrate brain. During early brain development, neural progenitors first expand their numbers through repeated proliferative divisions and then begin to exhibit neurogenic divisions. The transparent and experimentally accessible optic tectum of *Xenopus laevis* is an excellent model system for the study of the cell biology of neurogenesis, but the precise spatial and temporal relationship between proliferative and neurogenic progenitors has not been explored in this system. Here we construct a spatial map of proliferative and neurogenic divisions through lineage tracing of individual progenitors and their progeny. We find a clear spatial separation of proliferative and neurogenic progenitors along the anterior-posterior axis of the optic tectum, with proliferative progenitors located more posteriorly and neurogenic progenitors located more anteriorly. Since individual progenitors are repositioned toward more anterior locations as they mature, this spatial separation likely reflects an increased restriction in the proliferative potential of individual progenitors. We then examined whether the transition from proliferative to neurogenic behavior correlates with cellular properties that have previously been implicated in regulating neurogenesis onset. Our data reveal that the transition from proliferation to neurogenesis is associated with a small change in cleavage plane orientation and a more pronounced change in cell cycle kinetics in a manner reminiscent of observations from mammalian systems. Our findings highlight the potential to use the optic tectum of *Xenopus laevis* as an accessible system for the study of the cell biology of neurogenesis.

KEYWORDS

Neurogenesis, neural progenitor, cleavage plane orientation, cell cycle length, *Xenopus laevis*

INTRODUCTION

During vertebrate neurogenesis, progenitor cells are initially organized in a single layer of neuroepithelial cells that lines the brain ventricle. Progenitors display radial morphology with processes extending to both the pial and ventricular surfaces. In contrast, newborn neurons retract their radial processes, migrate away from the ventricular surface and start to develop neurites. Early during brain development, neural progenitors increase their numbers through repeated proliferative divisions. Later on, progenitors switch to neurogenic divisions. This transition must be finely tuned to ensure normal brain development (Taverna et al. 2014).

The external development and transparency of *Xenopus laevis* embryos makes them an ideal model system for studying brain development in real time, in a live and intact vertebrate. Time-lapse imaging has been used extensively to study certain aspects of neural development in the *Xenopus laevis* optic tectum, such as the formation of retinotectal synapses (Sanchez et al. 2006, Chiu et al. 2008, Schwartz et al. 2009, Chen et al. 2010, Li et al. 2011) and the development of dendritic morphology (Sin et al. 2002, Haas et al. 2006, Ewald et al. 2008, Van Keuren-Jensen and Cline 2008, Bestman and Cline 2008, Shen et al. 2009, Schwartz et al. 2009, Liu et al. 2009, Chen et al. 2010). However, much less is known about the cell biology of the tectal

progenitors that generate these neurons. While it has been shown that radial progenitor cells in the optic tectum can undergo both proliferative and neurogenic divisions, and that they can also differentiate directly into neurons (Bestman et al. 2012), the spatial and temporal relationship between proliferative and neurogenic progenitors has not been explored at the level of individual cells.

Given its importance for brain development and evolution, the regulation of the transition from proliferation to neurogenesis is a topic of great interest in neurobiology. Experimental evidence supports a role for a wide range of cell biological mechanisms in determining the fate of daughter cells from divisions of neural progenitors. These include, but are not limited to, the asymmetric inheritance of cell fate determinants, cell cycle kinetics, interkinetic nuclear migration, feedback signaling from neurons, and a number of extracellular signaling pathways (Willardsen and Link 2011, Paridaen and Huttner 2014, Taverna et al. 2014). Research in *Xenopus* has demonstrated that parameters such as visual activity (Sharma and Cline 2010), epigenetic modifications (Tao et al. 2015) and Fragile X Mental Retardation Protein expression (Faulkner et al. 2015) can play a role in the regulation of neurogenesis in the optic tectum. It is likely that these mechanisms cooperate and interact to influence cell fate, potentially over several cell cycles (Willardsen and Link 2011).

Here we explore the spatial and temporal relationship between proliferative and neurogenic progenitors in the developing optic tectum of *Xenopus laevis* through electroporation of individual neural progenitors, followed by lineage tracing of the progenitors and their progeny over several

days. We find that proliferative and neurogenic progenitors are spatially separated along the anterior-posterior axis of the optic tectum. Proliferative progenitors reside in the posterior tectum, while neurogenic progenitors are located more anteriorly. This separation of proliferative and neurogenic progenitors in space likely reflects the transition from proliferation to neurogenesis in time. In addition, we investigated the spatial distribution of cleavage plane orientation and cell cycle kinetics in neural progenitors - two cell biological parameters that have been proposed to play a role in cell fate determination during neurogenesis. Our data indicate that changes in both of these parameters are associated with the transition from proliferation to neurogenesis in tectal neural progenitors, with the change in cell cycle kinetics concomitant with neurogenesis onset being somewhat more pronounced than that in cleavage plane orientation.

METHODS

Animals

Wild-type *Xenopus laevis* tadpoles were reared on a 14 hour light/10 hour dark cycle at 15-21 °C in Modified Barth's Solution (MBS). Reagents were supplied by Sigma unless otherwise stated. To inhibit melanogenesis, the rearing solution also contained 100 μM N-Phenylthiourea. Tadpoles were staged according to established morphological criteria (Nieuwkoop and Faber 1994), and experiments were carried out between stages 45 and 48. All animal procedures were conducted in accordance with UK Home Office

regulations. Some animals were incubated in 10 mM BrdU in rearing solution for 2-30 hours before fixation and processing for immunohistochemistry.

Single-cell electroporation of tectal cells

We used single-cell electroporation of fluorescently labeled dextran to label individual radial and non-radial cells and characterize their neurogenic behavior (Haas et al. 2001, Bestman et al. 2006, Muldal et al. 2014, Herrgen et al. 2014). Animals were anaesthetized by immersion in MBS containing 0.01% Ethyl 3-aminobenzoate methansulfonate (MS-222). A glass micropipette containing 5 mg/ml Oregon Green 10,000 MW dextran (Life Technologies) in calcium-free Ringer's solution was positioned near or on the ventricular surface of the optic tectum. Cells were electroporated by delivering a short train of electrical pulses of 1-5 V using an Axoporator 800A (Molecular Devices). The labeling of individual cells was confirmed 1-3 hours after electroporation. Tadpoles with single cells were returned to rearing solution. They were then repeatedly imaged over 1-3 days, or allowed to develop for 1-3 days before fixation and processing for immunohistochemistry. To determine how individual progenitors change their positions relative to the heel and to each other over time, several cells were labeled within the same animal. Labeling was confirmed 1 hour after electroporation, and cells were repeatedly imaged over 3 days.

Nuclear and F-actin staining

Animals were euthanized in 2% MS-222 and fixed in 4% paraformaldehyde for 12-16 hours at 4 °C. After fixation, brains were excised, rinsed in

phosphate buffered saline (PBS), permeabilized for 1-4 hours at room temperature in PBS with 0.5% Triton X-100, rinsed in PBS and incubated in 50 μg/ml fluorescein isothiocyanate labeled phalloidin in PBS for 12-16 hours at 4 °C. Brains were then rinsed in PBS, incubated in PBS with 1 μg/ml propidium iodide (Invitrogen) and 100 μg/ml RNAse A (Roche) for 30 minutes at 37 °C and again rinsed in PBS before mounting and imaging.

Immunohistochemistry

Animals were euthanized in 2% MS-222 and fixed in 4% paraformaldehyde for 12-16 hours at 4 °C. After fixation, brains were excised, rinsed in PBS, blocked for 1-4 hours at room temperature in PBS with 1% BSA, 1% DMSO, 0.5% Triton X-100 and 0.01% sodium azide, and incubated in primary antibody in blocking solution for 12-16 hours at 4 °C. Primary antibodies used were mouse anti-HuC/D antibody (1:200, Life Technologies), mouse anti-BrdU antibody (1:500), and rabbit anti-phospho-histone H3 (Ser10) antibody (1:1000, Millipore). Brains were rinsed in PBS with 0.5% Triton X-100 for 2-4 hours at room temperature, incubated in secondary antibody in blocking solution for 12-16 hours at 4 °C, and rinsed in PBS. Secondary antibodies used were Alexa Fluor® 488 goat anti-mouse antibody (1:500, Life Technologies) and Alexa Fluor® 488 goat anti-rabbit antibody (1:500, Life Technologies). For detection of cell nuclei, brains were incubated in PBS with 1 μg/ml propidium iodide and 100 μg/ml RNAse A (Roche) for 30 minutes at 37 °C and rinsed in PBS before mounting and imaging.

Image acquisition and analysis

Images were collected on a confocal microscope with 488 nm and 543 nm lasers, a ×60 0.9 NA LUMPlanFl/IR objective (Olympus) and Fluoview FV300 image acquisition software (Olympus). Images were analyzed in ImageJ (http://rsbweb.nih.gov/ij) and figures were assembled in Adobe Illustrator (Adobe). In some images the contrast was varied across different parts of an individual cell, in order to facilitate visualization of both the cell body and the radial processes or neurites (Fig. 2). The position of the heel was defined as the most posterior-lateral point of the ventricular surface of the tectum, which in most animals is also the point of strongest inflection along the ventricular wall. The heel was assigned a value of 0 μm along the anterior-posterior axis of the optic tectum, with locations posterior and anterior to the heel being assigned negative and positive values, respectively.

To determine the apical-basal and anterior-posterior location of dividing cells, mitotic cells were visualized in z stacks of confocal images (1 μm intervals between optical planes) after staining for F-actin and cell nuclei. The position of each mitotic cell was identified manually and the cell's coordinates within the tectum were calculated using a custom-written script in MATLAB (Mathworks).

To track the behavior of individual radial cells labeled with fluorescent dextran, z stacks of confocal images (2 μm intervals between optical planes) were taken each day, for at least 3 days, starting on the day of electroporation. A cell's location on the anterior-posterior axis was measured as the distance along the ventricular wall, between the cell's apical endfoot and the heel.

To measure cleavage plane orientation, mitotic cells were visualized in z stacks of confocal images (1 μm intervals between optical planes), after staining for F-actin and cell nuclei. Only cells whose sister chromatids appeared similar in size and shape in consecutive optical sections were included in the analysis. The cleavage angle was calculated as the mean of the angles between each of the sister chromatids and the ventricular surface. A cell's location on the anterior-posterior axis was measured as the distance along the ventricular wall between the heel and the dividing cell. Based on the time-lapse imaging of individual progenitors, cells posterior to a position of 0 μm along the anterior-posterior axis were considered to reside in the proliferative region, while those anterior of this position were considered to be within the neurogenic region. A radial line from the heel through the tissue was defined as the boundary between the posterior and anterior parts of the optic tectum.

The spatial distribution of the early neuronal marker HuC/D$^+$ cells was investigated in z stacks of confocal images (2 μm intervals between optical planes), taken after staining for HuC/D and cell nuclei. The position of each HuC/D$^+$ cell was identified manually and the cell's coordinates within the tectum were calculated using a custom-written script in MATLAB.

To determine the BrdU labeling index and the proportion of cells in G2 phase or M phase, BrdU$^+$ or phospho-histone H3$^+$ cells were visualized in z stacks of confocal images (5 μm intervals between optical planes). The number of BrdU$^+$ or phospho-histone H3$^+$ cells, and the total number of cells (from cell nuclei staining), were determined manually in the most dorsal optical section that showed a clear outline of the ventricular wall.

Calculation of cell cycle phases

Calculation of the length of the cell cycle (T_C), the length of S phase (T_S), and the growth fraction (GF), which is the fraction of proliferating cells within a cell population, was performed by nonlinear regression analysis of cumulative BrdU labeling curves as described previously (Nowakowski et al. 1989) using an Excel spreadsheet kindly provided by Prof Richard S. Nowakowski. Briefly, the algorithm embedded in the spreadsheet calculates the intercept of the BrdU labeling curve with the y-axis (a), the time needed to reach maximum BrdU labeling (b), and GF through nonlinear regression. Importantly, the parameter a correlates with T_S/T_C, and the parameter b corresponds to $T_C - T_S$ (Nowakowski et al. 1989). Determining the parameters a, b, and GF by nonlinear regression analysis therefore allows us to solve the equations (T_S/T_C) GF = a and $T_C - T_S = b$, whereby we obtain T_C and T_S (Nowakowski et al. 1989).

We used phospho-histone H3 (Ser10) staining to determine the combined length of G2 phase and M phase (T_{G2+M}) based on reports that histone H3 is phosphorylated on serine 10 during G2 phase and M phase (Gurley et al. 1978, Paulson and Taylor 1982, Hendzel et al. 1997). We reasoned that the fraction of the total number of cells that stain for phospho-histone H3 would correspond to the fraction of the length of the cell cycle that cells spend in G2 phase and M phase. To obtain T_{G2+M} we therefore divided the number of phospho-histone $H3^+$ cells by the total number of cells in the population (calculated from cell nuclei staining) and then normalized this value by GF, to account for the existence of non-cycling cells within the population. The fraction we obtained was then multiplied by T_C to yield T_{G2+M}, and the

length of G1 phase (T_{G1}) was calculated by subtracting T_S and T_{G2+M} from T_C.

Statistical methods

All population data are presented as mean ± sem. Statistical tests were carried out as stated in the figure legends using Prism (GraphPad Software).

RESULTS

The majority of neural progenitors in the developing optic tectum of *Xenopus laevis* divides apically

The optic tectum is a major component of the midbrain in *Xenopus laevis* (Fig. 1A) and grows by addition of neurons from a posterior-lateral neuroepithelium (Straznicky and Gaze 1972, Lázár 1973). This neuroepithelium is located around the heel of the tectum, defined as the most posterior-lateral point along the ventricular surface, which is usually also the point of strongest inflection of the ventricular wall (Fig. 1B; see Methods). In the developing mammalian brain, neural progenitors can divide apically or basally within the neuroepithelium, and it is thought that apical and basal progenitors have different lineage potentials (Taverna et al. 2014). To investigate the existence of differentially localized pools of progenitors in the optic tectum, we stained cell nuclei and F-actin (Fig. 1C) and determined the apical-basal position of mitotic cells within the neuroepithelium (Fig. 1D). We found that 92% of dividing cells (49/53) were situated within one cell diameter of the ventricular surface, whereas the remaining 8% of cells (4/53) were located between one and two cell diameters away from the ventricular

surface. We did not detect any dividing cells (0/53) whose distance to the ventricular surface was greater than two cell diameters (n = 10 animals). These results show that the tectal progenitor pool is predominantly made up of progenitors that divide apically, at the ventricular surface. The small number of progenitors that does not divide apically nevertheless divides in close proximity to the ventricular surface.

Long-term *in vivo* time-lapse imaging can be used to trace individual neural progenitors and their progeny over several days

Next, we characterized tectal progenitors according to their neurogenic behavior. We used single-cell electroporation of fluorescently labeled dextran to label individual progenitors within the optic tectum. Electroporated cells were then followed over several days by long-term *in vivo* time-lapse imaging (Haas et al. 2001, Bestman et al. 2006). This allowed us to assess the fate of daughter cells from individual progenitors in the optic tectum (Muldal et al. 2014, Herrgen et al. 2014). We electroporated and followed a total of 49 tectal radial progenitors, which could exhibit four different types of behavior. We found that 29% of radial cells (14/49) underwent proliferative symmetric division (Fig. 2A-C), where one progenitor generates two progenitors. Radial cells could also exhibit one of three types of neurogenic behavior. We detected neurogenic asymmetric division, which gives rise to one progenitor and one neuron (Fig. 2D-F), in 16% of radial cells (8/49), and found that 29% of radial cells (14/49) underwent neurogenic symmetric division, which generates two neurons (Fig. 2G-I). In addition, we identified 26% of radial cells (13/49) as displaying direct neuronal differentiation, where a progenitor

becomes a neuron without dividing (Fig. 2J-L). Direct neuronal differentiation of radial cells has previously been observed in the *Xenopus* optic tectum (Bestman et al. 2012).

As we had detected a few progenitors that do not divide at the ventricular surface but slightly away from it (Fig. 1D), we were wondering whether these cells might be basal progenitors. To qualify as a basal progenitor, a cell needs to divide away from the ventricular wall, and also needs to have lost apical contact and therefore have become non-radial. To investigate whether we could detect any basal progenitors in the optic tectum, we delivered fluorescent dextrans to non-radial cells through single-cell electroporation (Fig. 2M) and then followed these cells over several days to determine whether they would divide (Fig. 2N,O). We found that 0% of non-radial cells (0/11) divided, whereas 100% of cells (11/11) started to develop neurites. These results suggest that all non-radial cells that we analyzed were newborn neurons rather than basal progenitors. Likewise, 0% of non-radial cells (0/8) generated by asymmetric divisions divided, while 100% of these cells (8/8) started to develop neurites, again indicating that these are newborn neurons. Taken together, we did not find evidence supporting the existence of a sizeable pool of basal progenitors in the optic tectum. Interestingly, even progenitors that did not divide directly on the ventricular surface resided no more than two cell diameters away from the ventricular surface, raising the possibility that they might be ectopically dividing apical progenitors.

Proliferative and neurogenic divisions are spatially separated in the developing optic tectum

By relating a cell's behavior to its anterior-posterior position relative to the heel on the day of electroporation, we were able to construct a map of progenitor cell behaviors in the optic tectum. Importantly, this revealed a clear spatial separation of proliferative and neurogenic behavior along the anterior-posterior axis (Fig. 3A). This spatial transition correlates closely with the location of the heel (Fig. 1B) and so to quantify the change from proliferative to neurogenic behavior, we defined the position of the heel as 0 μm along the anterior-posterior axis of the optic tectum. This confirmed that proliferative divisions occur at more posterior positions, whereas neurogenic divisions take place at more anterior positions within the neuroepithelium (Fig. 3B).

During development, the posterior margin of the tectum is displaced toward progressively more posterior locations as a result of tectal growth (Straznicky and Gaze 1972, Lázár 1973). Therefore, individual cells are repositioned toward more anterior locations relative to the heel over time, creating the impression that progenitors move in an anterior direction (Fig. 2). It is important to note that progenitors maintain their positions within the tissue and relative to each other during development despite this apparent movement. To directly confirm this, we electroporated several progenitors at different anterior-posterior locations and followed them and their progeny over several days (Fig. 4A-C). Indeed, this revealed that progenitors and their progeny are repositioned toward more anterior locations relative to the heel, while maintaining their positions relative to each other (Fig. 4D).

Given this anterior repositioning over time, it is likely that the spatial separation of proliferative divisions and neurogenic behavior reflects a progressive restriction in the proliferative potential of individual progenitors.

This means that at any particular stage of development, the maturational stage of a tectal progenitor is reflected by its position along the anterior-posterior axis of the tectum.

The transition from proliferative to neurogenic behavior is associated with the expression of the early neuronal marker HuC/D

We then investigated whether the transition from proliferative to neurogenic behavior identified by *in vivo* time-lapse imaging is recapitulated at the gene expression level. Using the early neuronal marker HuC/D, we did not detect any neurons in the proliferative region. However, HuC/D$^+$ newborn neurons were identified within the neurogenic region of the neuroepithelium (Fig. 5A,B). Indeed, the distribution of cells with neurogenic behavior closely paralleled the distribution of HuC/D$^+$ cells along the anterior-posterior axis of the neuroepithelium (Fig. 5C). The anterior shift of the HuC/D distribution relative to the distribution of cells with neurogenic behavior is consistent with anterior repositioning of newborn neurons relative to the heel as they start to differentiate and express HuC/D. To confirm the equivalence of results obtained from long-term *in vivo* time-lapse imaging and HuC/D staining at the level of individual cells, we assessed HuC/D expression in radial or non-radial cells labeled by single-cell electroporation (Fig. 5D). This revealed that 0% of radial cells (0/23) but 100% of non-radial cells (14/14) expressed HuC/D (Fig. 5E). The strong correlation between these parameters ($n = 9$ animals, $p < 0.01$ in Fisher's exact test) confirmed that HuC/D expression recapitulates neurogenic behavior as assessed by long-term *in vivo* time-lapse imaging.

Mapping the spatial distribution of cleavage plane orientation shows that cleavage angles vary along the anterior-posterior axis

To further characterize neurogenesis in the *Xenopus laevis* optic tectum, we were keen to explore the spatial distribution of cell biological parameters that have previously been associated with the onset of neurogenesis. One such parameter is the orientation of the cleavage plane in dividing progenitors. Planar divisions, in which the cleavage plane is oriented between 60º and 90º to the ventricular surface, are believed to be symmetric and generate two identical daughters - either progenitors or neurons. Conversely, oblique or vertical divisions, in which the cleavage plane is between 0º and 60º, are believed to be asymmetric and produce one progenitor and one neuron (Chenn and McConnell 1995). This causal relationship was proposed to originate from equal or unequal partitioning of cell fate determinants that are differentially distributed along a cell's apical-basal axis (Kosodo et al. 2004). Consistent with this, the overall number of vertical divisions increases during neurogenesis (Haydar et al. 2003).

We were interested to see whether any correlation exists between the spatial distribution of cleavage angles and the spatial distribution of proliferative and neurogenic progenitors in the optic tectum. We measured cleavage angles in brains stained for cell nuclei and F-actin and found that they ranged from 0º to 90º (Fig. 6A-D). Almost all divisions in the proliferative region of the optic tectum were planar (Fig. 6E,F). Most divisions in the neurogenic region were also planar, however we did detect an increase in the proportion of oblique and vertical divisions (Fig. 6E,F). Interestingly, the location of the first oblique and vertical divisions correlated with the spatial

position of the first neurogenic divisions (Fig. 6E). Taken together, these data show that while the onset of neurogenesis is associated with a small increase in oblique and vertical divisions, most progenitors undergo planar divisions irrespective of their location along the anterior-posterior axis of the optic tectum.

Mapping cell cycle parameters shows that cell cycle length is dynamically regulated along the anterior-posterior axis

Another model that has been put forward to account for the transition from proliferation to neurogenesis is the so-called cell cycle length hypothesis, which postulates that the length of the G1 phase of the cell cycle can influence cell fate choice (Calegari and Huttner 2003, Borrell and Calegari 2014, Hardwick et al. 2015). This hypothesis was initially based on the observation that T_{G1} increases as development proceeds and more progenitors transition from proliferation to neurogenesis (Takahashi et al. 1995). Consistent with this, progenitors in brain regions with a higher proportion of neurogenic divisions display a longer G1 phase (Lukaszewicz et al. 2005), and neurogenic progenitors are characterized by a longer G1 phase than proliferative progenitors within the same brain region (Calegari et al. 2005).

To investigate whether there are any changes in cell cycle kinetics that correlate with the spatial separation of proliferative and neurogenic progenitors, we compared cell cycle parameters in the proliferative and neurogenic regions of the developing optic tectum. The length of the cell cycle and the length of S phase can be calculated using cumulative BrdU labeling

(Nowakowski et al. 1989). Animals were incubated in the presence of BrdU for varying amounts of time (Fig. 7A-H). We then determined the proportion of $BrdU^+$ cells within proliferative and neurogenic regions at different time points, and calculated T_C and T_S from the resulting cumulative labeling curves (Fig. 7I; see Methods). We found that T_C was longer in the neurogenic region than in the proliferative region, while T_S was shorter (Fig. 7J). Our measurements indicated that T_C in the neurogenic region is approximately 25 hours, which is consistent with previous results from the anterior optic tectum of *Xenopus* (Sharma and Cline 2010). To determine T_{G2+M}, we used phospho-histone H3 immunostaining (Fig. 7K,L; see Methods). Histone H3 is phosphorylated on serine 10 during G2 phase and M phase (Gurley et al. 1978, Paulson and Taylor 1982, Hendzel et al. 1997). Therefore, the ratio of the number of phospho-histone $H3^+$ cells to the total number of proliferating cells reflects the ratio of T_{G2+M} to T_C. We found that the length of T_{G2+M} did not differ between the proliferative and neurogenic regions. In combination, these results allowed us to estimate the length of T_{G1}, which revealed that T_{G1} was more than twice as long in the neurogenic region compared to the proliferative region (Fig. 7M; see Methods). These results suggest that cell cycle parameters vary dynamically along the anterior-posterior axis of the optic tectum.

DISCUSSION

The timing of the transition from proliferative to neurogenic divisions in neural progenitors determines the number of neurons in the mature brain. Premature

neurogenesis onset underlies developmental disorders such as microcephaly (Barbelanne and Tsang 2014). Conversely, delayed neurogenesis onset in higher organisms may have contributed to the evolution of complex brain structures (Rakic 1995).

We explored the transition from proliferation to neurogenesis in the developing optic tectum of *Xenopus laevis* embryos, whose external development and transparency makes them ideally suited for analysis of the cell biology of neurogenesis, in particular for lineage tracing through long-term live imaging. We exploited these advantages to construct a spatial map of the neurogenic behavior of tectal progenitors. We found a boundary in space along the anterior-posterior axis, which separates proliferative progenitors in the posterior tectum from neurogenic progenitors in the anterior tectum. This likely reflects the transition from proliferation to neurogenesis in time because individual progenitors are repositioned relative to the heel toward more anterior locations as they develop and mature (Fig. 4). Therefore, the spatial position of a tectal progenitor can be used as an indicator of its maturational state. We first identified this boundary by mapping the proliferative behavior of neural progenitors onto their spatial location through long-term *in vivo* time lapse imaging of individual progenitors over several days. We then confirmed that this boundary also manifests at the population level, as shown by HuC/D expression.

Given the clear spatial separation of proliferative and neurogenic progenitors, we were keen to explore whether any cell biological parameters that have been proposed to play a role in the regulation of neurogenesis onset would also vary along the anterior-posterior axis of the tectum. One such

parameter is the orientation of the cleavage plane in dividing progenitors, which has been proposed to generate symmetric or asymmetric cell fates through the equal or unequal partitioning of fate determinants (Kosodo et al. 2004). Indeed, we found that the transition from proliferative to neurogenic divisions is associated with an increase in oblique and vertical divisions (Fig. 6E,F). Nonetheless, the majority of divisions across the optic tectum was found to be planar. In particular, more than 95% of divisions in the neurogenic region generated at least one neuron (Fig. 3), but only 18% of divisions displayed vertical or oblique cleavage angles (Fig. 6E,F). This indicates that while oblique or vertical orientation of the cleavage plane in dividing neural progenitors may be one of the factors contributing to neurogenesis onset in the optic tectum, this does not appear to be a requirement for the majority of neurogenic divisions.

Another mechanism that has been implicated in regulating the transition from proliferative to neurogenic divisions is an increase in T_{G1}. The underlying mechanism has been proposed to be the accumulation of cell fate-determining differentiation factors, which will only accumulate to levels high enough to induce neurogenesis if a cell's G1 phase is longer than a certain threshold value (Calegari and Huttner 2003, Borrell and Calegari 2014, Hardwick et al. 2015). To determine whether there is any association between the length of different phases of the cell cycle and neurogenesis onset in the optic tectum, we calculated T_C, T_S, T_{G2+M} and T_{G1} in the proliferative and neurogenic regions through cumulative BrdU labeling and phospho-histone H3 immunostaining. We found that T_C and T_{G1} were longer in the neurogenic region, T_S was shorter, and we did not detect a difference in the length of

T_{G2+M} (Fig. 7J,M). These findings establish an association between the proliferative behavior of neural progenitor cells in the optic tectum and the length of different phases of their cell cycle. Indeed, the increase in T_{G1} in neurogenic progenitors is reminiscent of the correlation between T_{G1} and a progenitor's maturational state that has been observed in mammalian systems (Takahashi et al. 1995, Calegari et al. 2005, Lukaszewicz et al. 2005). In addition, the decrease in T_S in neurogenic progenitors as compared to proliferative progenitors that we detected in the optic tectum (Fig. 7J) parallels a similar decrease reported in mammalian systems (Arai et al. 2011). This decrease in T_S has been proposed to reflect the increase in time that proliferative progenitors invest in quality control of DNA replication.

In conclusion, by constructing a map of the distribution of proliferative and neurogenic progenitors in the optic tectum of *Xenopus laevis* using *in vivo* imaging methods, we show that the spatial and temporal relationship between progenitors with different proliferative potential can be mapped at the level of individual cells in this system. Our observations also indicate that a small change in cleavage plane orientation and a more marked difference in cell cycle kinetics accompany neurogenesis onset in the optic tectum of *Xenopus laevis*, reminiscent of findings from the developing mammalian brain. Therefore, our findings provide further evidence that the *Xenopus* optic tectum represents a simple and tractable model system in which to investigate the cell biology underlying vertebrate neurogenesis.

We thank Prof Richard S. Nowakowski for kindly providing the Excel spreadsheet for calculation of cell cycle parameters, and members of the Akerman lab for helpful discussions and comments on the manuscript. This work was supported by grants from the Biotechnology

and Biological Sciences Research Council (BB/E0154761) and the European Research Council under the European Community's Seventh Framework Programme, ERC grant agreement numbers 243273 and 617670. L.H. was supported by a European Blaschko Visiting Research Fellowship and an EMBO Long-Term Fellowship (ALTF 1076-2010). The authors declare no competing financial interests.

REFERENCES

Arai Y, Pulvers JN, Haffner C, Schilling B, Nüsslein I, Calegari F, Huttner WB. 2011. Neural stem and progenitor cells shorten S-phase on commitment to neuron production. Nat Commun 2:154.

Barbelanne M, Tsang WY. 2014. Molecular and cellular basis of autosomal recessive primary microcephaly. Biomed Res Int 2014:547986.

Bestman JE, Cline HT. 2008. The RNA binding protein CPEB regulates dendrite morphogenesis and neuronal circuit assembly in vivo. Proc Natl Acad Sci USA 105:20494–99.

Bestman JE, Ewald RC, Chiu S-L, Cline HT. 2006. In vivo single-cell electroporation for transfer of DNA and macromolecules. Nature Protocols 1:1267–72.

Bestman JE, Lee-Osbourne J, Cline HT. 2012. In vivo time-lapse imaging of cell proliferation and differentiation in the optic tectum of Xenopus laevis tadpoles. J Comp Neurol 520:401–33.

Borrell V, Calegari F. 2014. Mechanisms of brain evolution: regulation of neural progenitor cell diversity and cell cycle length. Neurosci Res 86:14–24.

Calegari F, Haubensak W, Haffner C, Huttner WB. 2005. Selective lengthening of the cell cycle in the neurogenic subpopulation of neural progenitor cells during mouse brain development. J Neurosci 25:6533–38.

Calegari F, Huttner WB. 2003. An inhibition of cyclin-dependent kinases that lengthens, but does not arrest, neuroepithelial cell cycle induces premature neurogenesis. J Cell Sci 116:4947–55.

Chen SX, Tari PK, She K, Haas K. 2010. Neurexin-neuroligin cell adhesion

complexes contribute to synaptotropic dendritogenesis via growth stabilization mechanisms in vivo. Neuron 67:967–83.

Chenn A, McConnell SK. 1995. Cleavage orientation and the asymmetric inheritance of Notch1 immunoreactivity in mammalian neurogenesis. Cell 82:631–41.

Chiu S-L, Chen C-M, Cline HT. 2008. Insulin receptor signaling regulates synapse number, dendritic plasticity, and circuit function in vivo. Neuron 58:708–19.

Ewald RC, Van Keuren-Jensen KR, Aizenman CD, Cline HT. 2008. Roles of NR2A and NR2B in the development of dendritic arbor morphology in vivo. J Neurosci 28:850–61.

Faulkner RL, Wishard TJ, Thompson CK, Liu H-H, Cline HT. 2015. FMRP regulates neurogenesis in vivo in Xenopus laevis tadpoles. eNeuro 2:e0055.

Gurley LR, D'Anna JA, Barham SS, Deaven LL, Tobey RA. 1978. Histone phosphorylation and chromatin structure during mitosis in Chinese hamster cells. Eur J Biochem 84:1–15.

Haas K, Li J, Cline HT. 2006. AMPA receptors regulate experience-dependent dendritic arbor growth in vivo. Proc Natl Acad Sci USA 103:12127–31.

Haas K, Sin W-C, Javaherian A, Li Z, Cline HT. 2001. Single-Cell Electroporation for Gene Transfer In Vivo. Neuron 29:583–91.

Hardwick LJA, Ali FR, Azzarelli R, Philpott A. 2015. Cell cycle regulation of proliferation versus differentiation in the central nervous system. Cell Tissue Res 359:187–200.

Haydar TF, Ang E, Rakic P. 2003. Mitotic spindle rotation and mode of cell

division in the developing telencephalon. Proc Natl Acad Sci USA 100:2890–95.

Hendzel MJ, Wei Y, Mancini MA, Van Hooser A, Ranalli T, Brinkley BR, Bazett-Jones DP, Allis CD. 1997. Mitosis-specific phosphorylation of histone H3 initiates primarily within pericentromeric heterochromatin during G2 and spreads in an ordered fashion coincident with mitotic chromosome condensation. Chromosoma 106:348–60.

Herrgen L, Voss OP, Akerman CJ. 2014. Calcium-dependent neuroepithelial contractions expel damaged cells from the developing brain. Dev Cell 31:599–613.

Kosodo Y, Röper K, Haubensak W, Marzesco A-M, Corbeil D, Huttner WB. 2004. Asymmetric distribution of the apical plasma membrane during neurogenic divisions of mammalian neuroepithelial cells. EMBO J 23:2314–24.

Lázár G. 1973. The development of the optic tectum in Xenopus laevis: a Golgi study. J Anat 116:347–55.

Li J, Erisir A, Cline H. 2011. In vivo time-lapse imaging and serial section electron microscopy reveal developmental synaptic rearrangements. Neuron 69:273–86.

Liu XF, Tari PK, Haas K. 2009. PKM zeta restricts dendritic arbor growth by filopodial and branch stabilization within the intact and awake developing brain. J Neurosci 29:12229–35.

Lukaszewicz A, Savatier P, Cortay V, Giroud P, Huissoud C, Berland M, Kennedy H, Dehay C. 2005. G1 phase regulation, area-specific cell cycle control, and cytoarchitectonics in the primate cortex. Neuron 47:353–64.

Muldal AM, Lillicrap TP, Richards BA, Akerman CJ. 2014. Clonal relationships impact neuronal tuning within a phylogenetically ancient vertebrate brain structure. Curr Biol 24:1929–33.

Nieuwkoop PD, Faber J. 1994. Normal Table of Xenopus laevis (Daudin). Garland Publishing, New York.

Nowakowski RS, Lewin SB, Miller MW. 1989. Bromodeoxyuridine immunohistochemical determination of the lengths of the cell cycle and the DNA-synthetic phase for an anatomically defined population. J Neurocytol 18:311–18.

Paridaen JTML, Huttner WB. 2014. Neurogenesis during development of the vertebrate central nervous system. EMBO Reports 15:351–64.

Paulson JR, Taylor SS. 1982. Phosphorylation of histones 1 and 3 and nonhistone high mobility group 14 by an endogenous kinase in HeLa metaphase chromosomes. J Biol Chem 257:6064–72.

Rakic P. 1995. A small step for the cell, a giant leap for mankind: a hypothesis of neocortical expansion during evolution. Trends Neurosci 18:383–88.

Sanchez AL, Matthews BJ, Meynard MM, Hu B, Javed S, Cohen Cory S. 2006. BDNF increases synapse density in dendrites of developing tectal neurons in vivo. Development 133:2477–86.

Schwartz N, Schohl A, Ruthazer ES. 2009. Neural activity regulates synaptic properties and dendritic structure in vivo through calcineurin/NFAT signaling. Neuron 62:655–69.

Sharma P, Cline HT. 2010. Visual activity regulates neural progenitor cells in developing Xenopus CNS through musashi1. Neuron 68:442–55.

Shen W, Da Silva JS, He H, Cline HT. 2009. Type A GABA-receptor-

dependent synaptic transmission sculpts dendritic arbor structure in Xenopus tadpoles in vivo. J Neurosci 29:5032–43.

Sin W-C, Haas K, Ruthazer ES, Cline HT. 2002. Dendrite growth increased by visual activity requires NMDA receptor and Rho GTPases. Nature 419:475–80.

Straznicky K, Gaze RM. 1972. The development of the tectum in Xenopus laevis: an autoradiographic study. J Embryol Exp Morphol 28:87–115.

Takahashi T, Nowakowski RS, Caviness VS. 1995. The cell cycle of the pseudostratified ventricular epithelium of the embryonic murine cerebral wall. J Neurosci 15:6046–57.

Tao Y, Ruan H, Guo X, Li L, Shen W. 2015. HDAC1 regulates the proliferation of radial glial cells in the developing Xenopus tectum. PLoS ONE 10:e0120118.

Taverna E, Götz M, Huttner WB. 2014. The cell biology of neurogenesis: toward an understanding of the development and evolution of the neocortex. Annu Rev Cell Dev Biol 30:465–502.

Van Keuren-Jensen KR, Cline HT. 2008. Homer proteins shape Xenopus optic tectal cell dendritic arbor development in vivo. Dev Neurobiol 68:1315–24.

Willardsen MI, Link BA. 2011. Cell biological regulation of division fate in vertebrate neuroepithelial cells. Dev Dyn 240:1865–79.

FIGURE LEGENDS

Figure 1 The optic tectum of *Xenopus laevis* develops from a neuroepithelium where the great majority of progenitors divides apically. (A) Head of a stage 48 *Xenopus laevis*. FB, forebrain. MB, midbrain. HB, hindbrain. OT, optic tectum. Scale bar represents 200 μm. (B) The posterior-lateral region of the optic tectum comprises a neuroepithelium. NE, neuroepithelium. P, pia. V, ventricle. Scale bar represents 10 μm. (C) Mitotic cells (dashed circle) can be identified after staining for F-actin (green) and cell nuclei (magenta). Scale bar represents 10 μm. (D) Summary diagram showing the localization of mitotic cells. n = 10 animals. Scale bar represents 10 μm.

Figure 2 Single-cell *in vivo* time-lapse imaging of neural progenitors reveals four different types of progenitor cell behavior. Each row of the figure comprises three panels showing an animal's left optic tectum on consecutive days. The first image in each row was taken 1-3 h after single-cell electroporation. (A-C) A radial progenitor electroporated with fluorescent dextran (A) undergoes a proliferative symmetric division and generates two radial progenitor cells (B), and further divisions produce four cells (C). Scale bars in main panel and inset represent 10 μm and 5 μm, respectively. (D-F) A radial progenitor cell (D) undergoes a neurogenic asymmetric division, which generates another radial progenitor and a non-radial neuron (E). The newborn neuron subsequently migrates away from the ventricular surface (F). (G-I) A radial progenitor (G) undergoes a neurogenic symmetric division and

generates two non-radial neurons. The newborn neurons then migrate away from the ventricular surface (H) and develop neurites (I). (J-K) A radial progenitor cell (J) undergoes direct neuronal differentiation by retracting its radial processes (K) and developing neurites (L). (M-O) A non-radial cell (M) does not divide over several days but instead moves away from the ventricular surface (N) and starts to develop neurites (O).

Figure 3 Proliferative and neurogenic progenitors are spatially separated along the anterior-posterior axis of the developing optic tectum. (A) Progenitors in the posterior part of the tectum undergo proliferative divisions, whereas those located more anteriorly generate neurons. The positions of cell bodies indicate the apical-basal extent of the neuroepithelium. PD, proliferative division. ND, neurogenic division. DD, direct neuronal differentiation. n = 42 animals. Scale bar represents 10 μm. (B) Quantification of the prevalence of different types of cell behavior within 20 μm bins along the ventricular wall. The vertical dashed line indicates the boundary between regions of proliferative and neurogenic behavior. P, proliferative. N, neurogenic.

Figure 4 Tectal progenitors and their progeny are repositioned relative to the heel during development. (A-C) The positions of four radial progenitors (A) and their progeny relative to the heel change as they divide (B) and mature (C), while their positions relative to each other are maintained. Scale bar represents 10 μm. (D) Measurement of the positions of the individual progenitors and their progeny in (A-C) relative to the heel over three days.

Figure 5 The expression pattern of HuC/D within the neuroepithelium parallels the spatial distribution of neurogenic progenitors. (A) The optic tectum stained for HuC/D (green) and cell nuclei (magenta). The most posteriorly located HuC/D$^+$ cells (arrowheads) are found near the pial surface of the neuroepithelium. The vast majority of HuC/D$^+$ cells resides in the neuronal layer, which overlies the neuroepithelium in the anterior tectum. Scale bar represents 10 μm. (B) HuC/D immunoreactivity from the image shown in (A). (C) Quantification of the distribution of neurogenic progenitors as assessed by *in vivo* time-lapse imaging, and quantification of the distribution of HuC/D$^+$ cells, along the anterior-posterior axis of the neuroepithelium. n = 42 and 41 animals for *in vivo* time-lapse imaging and HuC/D staining, respectively. (D) The optic tectum stained for HuC/D after electroporation. The panel is a composite of two images from two different animals. Scale bar represents 10 μm. (E) The radial cell does not express HuC/D (filled arrowheads), whereas all four non-radial cells express HuC/D (open arrowheads). SCE, single-cell electroporation. Scale bar represents 10 μm.

Figure 6 Neural progenitor divisions are predominantly planar but oblique and vertical divisions are increased in the neurogenic region of the optic tectum. (A,C) The optic tectum stained for F-actin (green) and cell nuclei (magenta), revealing planar (A) and vertical (C) progenitor divisions. Scale bar represents 5 μm. (B,D) Higher magnification images of the dividing cells in (A) and (C). Scale bar represents 2 μm. (E) Distribution of cleavage angle orientation along the anterior-posterior axis of the optic tectum.

n = 76 animals. (F) The majority of divisions are planar, although there is an increase in the proportion of oblique and vertical divisions in the neurogenic region. *, $p < 0.05$ in Fisher's exact test.

Figure 7 The length of the cell cycle, S phase and G1 phase differ between proliferative and neurogenic regions of the optic tectum. (A-D) The optic tectum stained for BrdU (green) and cell nuclei (magenta) after 2 hours (A), 6 hours (B), 14 hours (C) and 30 hours (D) of incubation with BrdU. P, proliferative region. N, neurogenic region. Scale bar represents 10 μm. (E-H) BrdU immunoreactivity from the images shown in (A-D). (I) Quantification of the fraction of $BrdU^+$ cells over time in the proliferative and neurogenic regions. n = 22 animals. (J) Length of cell cycle (left) and length of S phase (right) in proliferative and neurogenic regions. (K) The optic tectum stained for phospho-histone H3 (green) and cell nuclei (magenta). Phospho-histone $H3^+$ cells (arrowheads) exhibited clear somatic labeling and reside near the ventricular wall. In contrast, staining in the neuronal region is not associated with cell somata. n = 6 animals. Scale bar represents 10 μm. (L) Phospho-histone H3 immunoreactivity from the image shown in (K). (M) Combined length of G2 phase and M phase (left) and length of G1 phase (right) in proliferative and neurogenic regions. All population data are displayed as mean ± sem. **, $p < 0.01$ in unpaired t-test with Welch's correction.

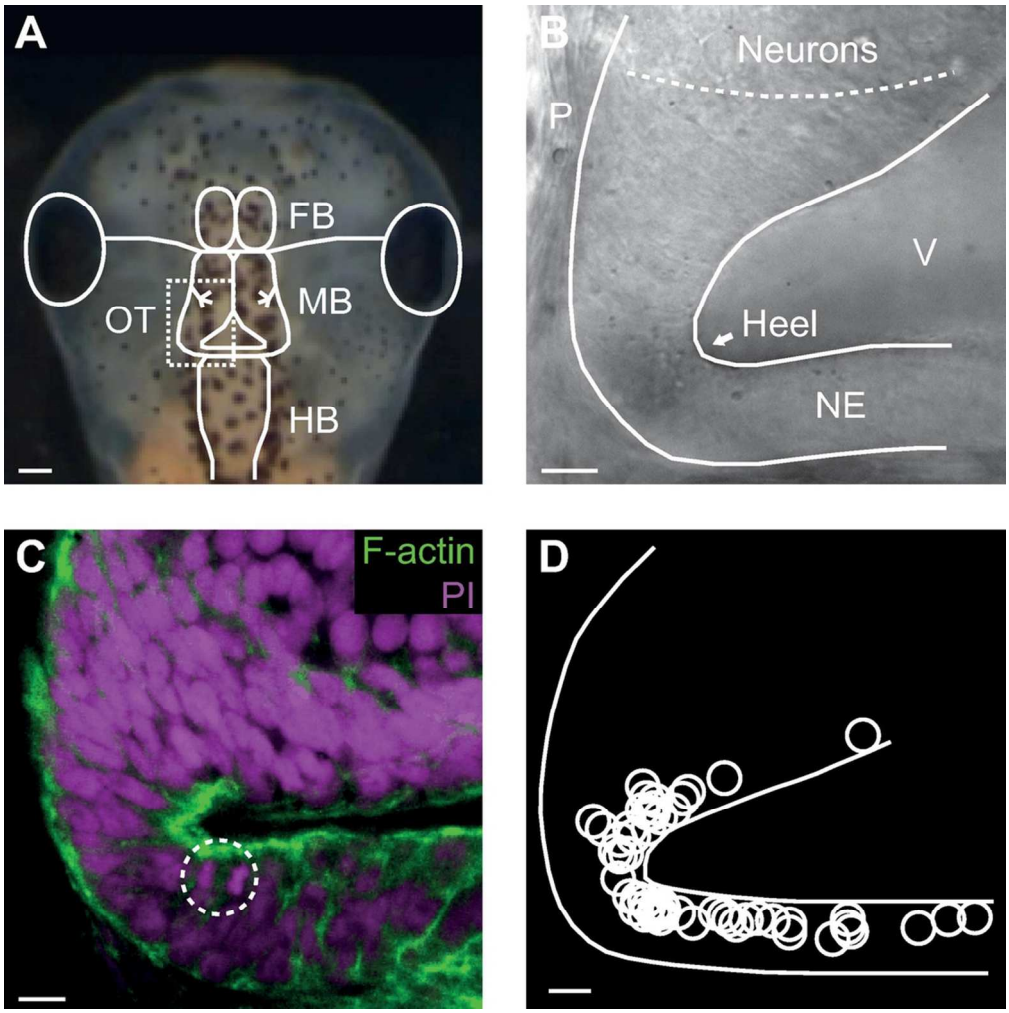

Figure 1 The optic tectum of Xenopus laevis develops from a neuroepithelium where the great majority of progenitors divides apically. (A) Head of a stage 48 Xenopus laevis. FB, forebrain. MB, midbrain. HB, hindbrain. OT, optic tectum. Scale bar represents 200 μm. (B) The posterior-lateral region of the optic tectum comprises a neuroepithelium. NE, neuroepithelium. P, pia. V, ventricle. Scale bar represents 10 μm. (C) Mitotic cells (dashed circle) can be identified after staining for F-actin (green) and cell nuclei (magenta). Scale bar represents 10 μm. (D) Summary diagram showing the localization of mitotic cells. n = 10 animals. Scale bar represents 10 μm.
94x94mm (300 x 300 DPI)

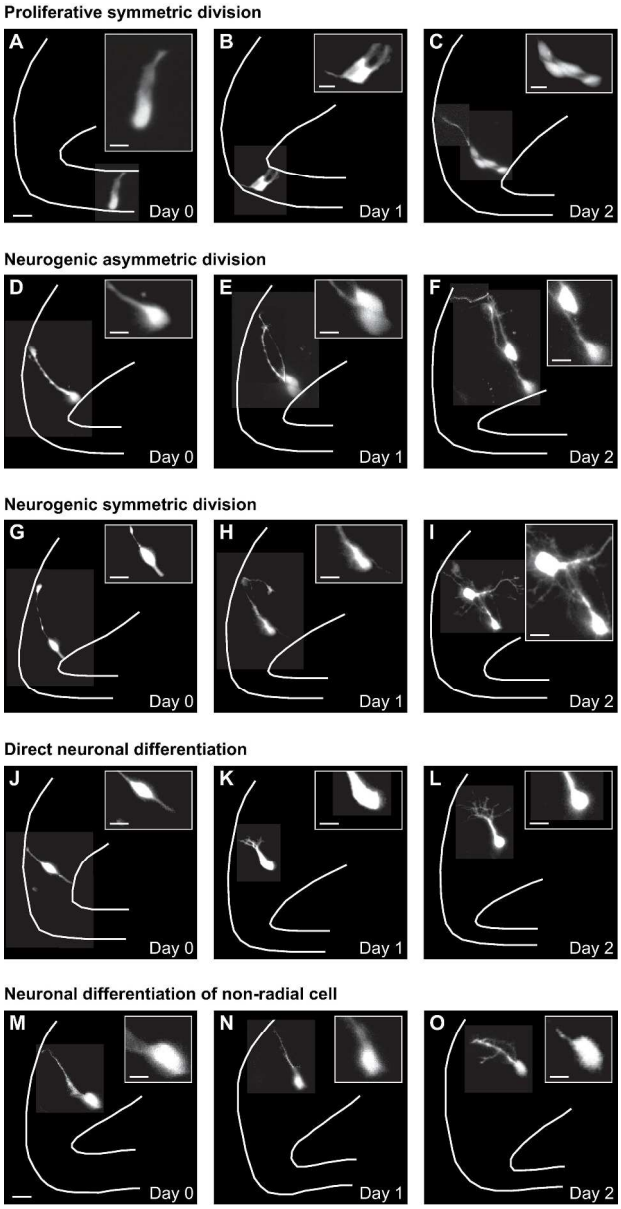

Figure 2 Single-cell in vivo time-lapse imaging of neural progenitors reveals four different types of progenitor cell behavior. Each row of the figure comprises three panels showing an animal's left optic tectum on consecutive days. The first image in each row was taken 1-3 h after single-cell electroporation. (A-C) A radial progenitor electroporated with fluorescent dextran (A) undergoes a proliferative symmetric division and generates two radial progenitor cells (B), and further divisions produce four cells (C). Scale bars in main panel and inset represent 10 μm and 5 μm, respectively. (D-F) A radial progenitor cell (D) undergoes a neurogenic asymmetric division, which generates another radial progenitor and a non-radial neuron (E). The newborn neuron subsequently migrates away from the ventricular surface (F). (G-I) A radial progenitor (G) undergoes a neurogenic symmetric division and generates two non-radial neurons. The newborn neurons then migrate away from the ventricular surface (H) and develop neurites (I). (J-K) A radial progenitor cell (J) undergoes direct neuronal differentiation by retracting its radial processes (K) and developing neurites (L). (M-O) A non-radial cell (M) does not divide over several days but instead moves away from the ventricular surface (N) and starts to develop neurites (O).

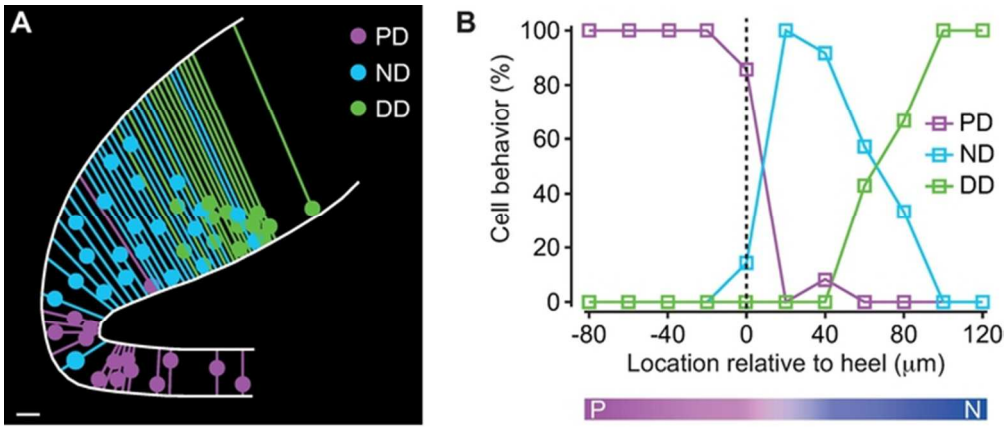

Figure 3 Proliferative and neurogenic progenitors are spatially separated along the anterior-posterior axis of the developing optic tectum. (A) Progenitors in the posterior part of the tectum undergo proliferative divisions, whereas those located more anteriorly generate neurons. The positions of cell bodies indicate the apical-basal extent of the neuroepithelium. PD, proliferative division. ND, neurogenic division. DD, direct neuronal differentiation. n = 42 animals. Scale bar represents 10 μm. (B) Quantification of the prevalence of different types of cell behavior within 20 μm bins along the ventricular wall. The vertical dashed line indicates the boundary between regions of proliferative and neurogenic behavior. P, proliferative. N, neurogenic.
60x25mm (300 x 300 DPI)

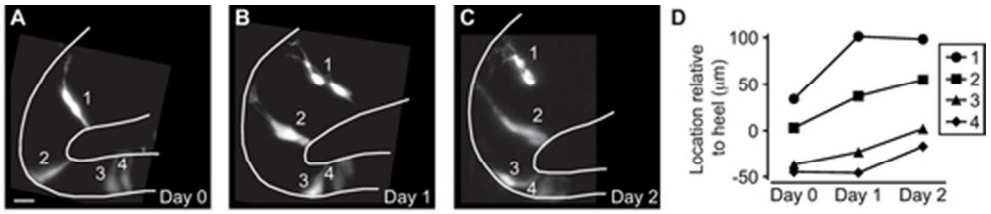

Figure 4 Tectal progenitors and their progeny are repositioned relative to the heel during development. (A-C) The positions of four radial progenitors (A) and their progeny relative to the heel change as they divide (B) and mature (C), while their positions relative to each other are maintained. Scale bar represents 10 μm. (D) Measurement of the positions of the individual progenitors and their progeny in (A-C) relative to the heel over three days.
45x10mm (300 x 300 DPI)

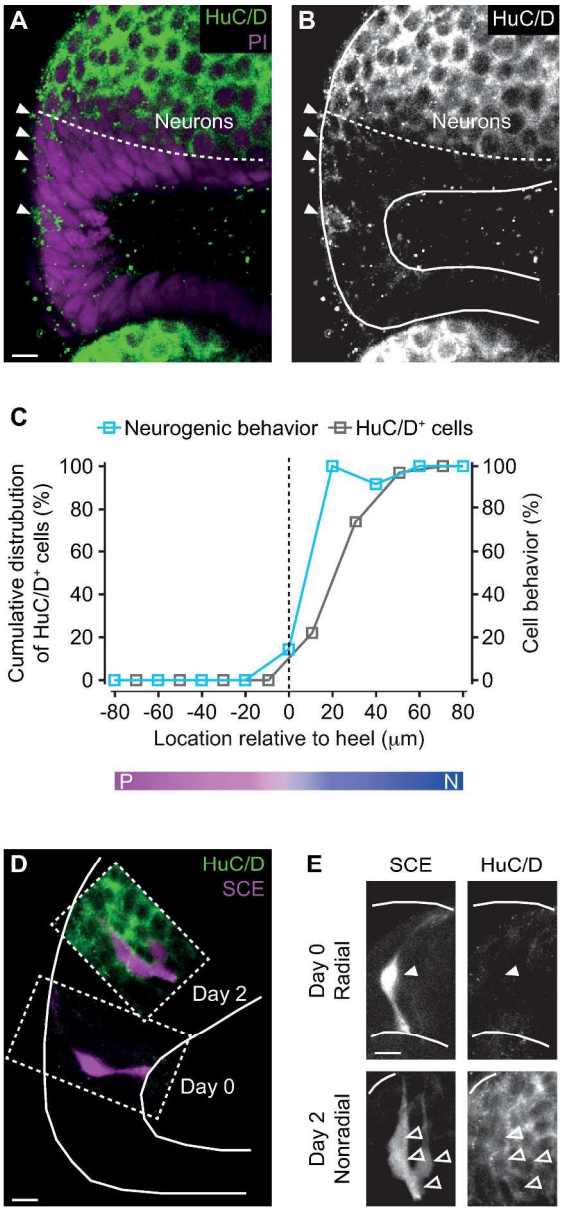

Figure 5 The expression pattern of HuC/D within the neuroepithelium parallels the spatial distribution of neurogenic progenitors. (A) The optic tectum stained for HuC/D (green) and cell nuclei (magenta). The most posteriorly located HuC/D+ cells (arrowheads) are found near the pial surface of the neuroepithelium. The vast majority of HuC/D+ cells resides in the neuronal layer, which overlies the neuroepithelium in the anterior tectum. Scale bar represents 10 μm. (B) HuC/D immunoreactivity from the image shown in (A). (C) Quantification of the distribution of neurogenic progenitors as assessed by in vivo time-lapse imaging, and quantification of the distribution of HuC/D+ cells, along the anterior-posterior axis of the neuroepithelium. n = 42 and 41 animals for in vivo time-lapse imaging and HuC/D staining, respectively. (D) The optic tectum stained for HuC/D after electroporation. The panel is a composite of two images from two different animals. Scale bar represents 10 μm. (E) The radial cell does not express HuC/D (filled arrowheads), whereas all four non-radial cells express HuC/D (open arrowheads). SCE, single-cell electroporation. Scale bar represents 10 μm.
201x417mm (300 x 300 DPI)

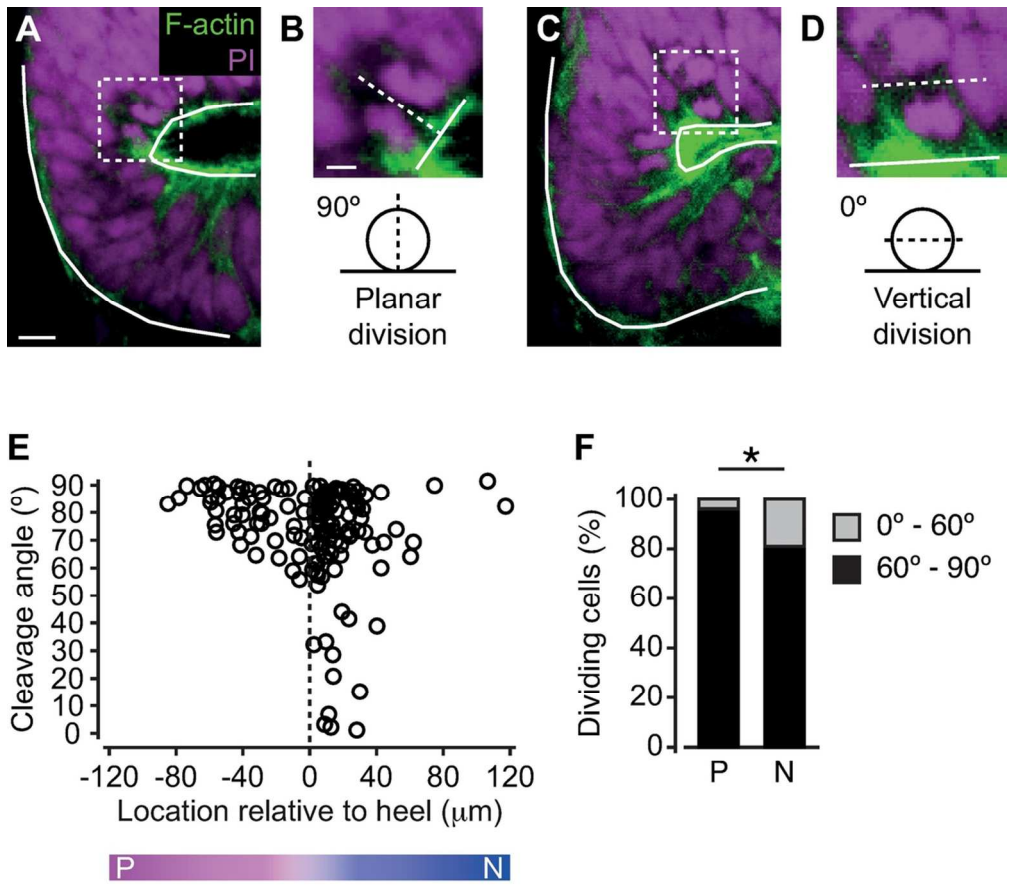

Figure 6 Neural progenitor divisions are predominantly planar but oblique and vertical divisions are increased in the neurogenic region of the optic tectum. (A,C) The optic tectum stained for F-actin (green) and cell nuclei (magenta), revealing planar (A) and vertical (C) progenitor divisions. Scale bar represents 5 μm. (B,D) Higher magnification images of the dividing cells in (A) and (C). Scale bar represents 2 μm. (E) Distribution of cleavage angle orientation along the anterior-posterior axis of the optic tectum. n = 76 animals. (F) The majority of divisions are planar, although there is an increase in the proportion of oblique and vertical divisions in the neurogenic region. *, $p < 0.05$ in Fisher's exact test.
103x91mm (300 x 300 DPI)

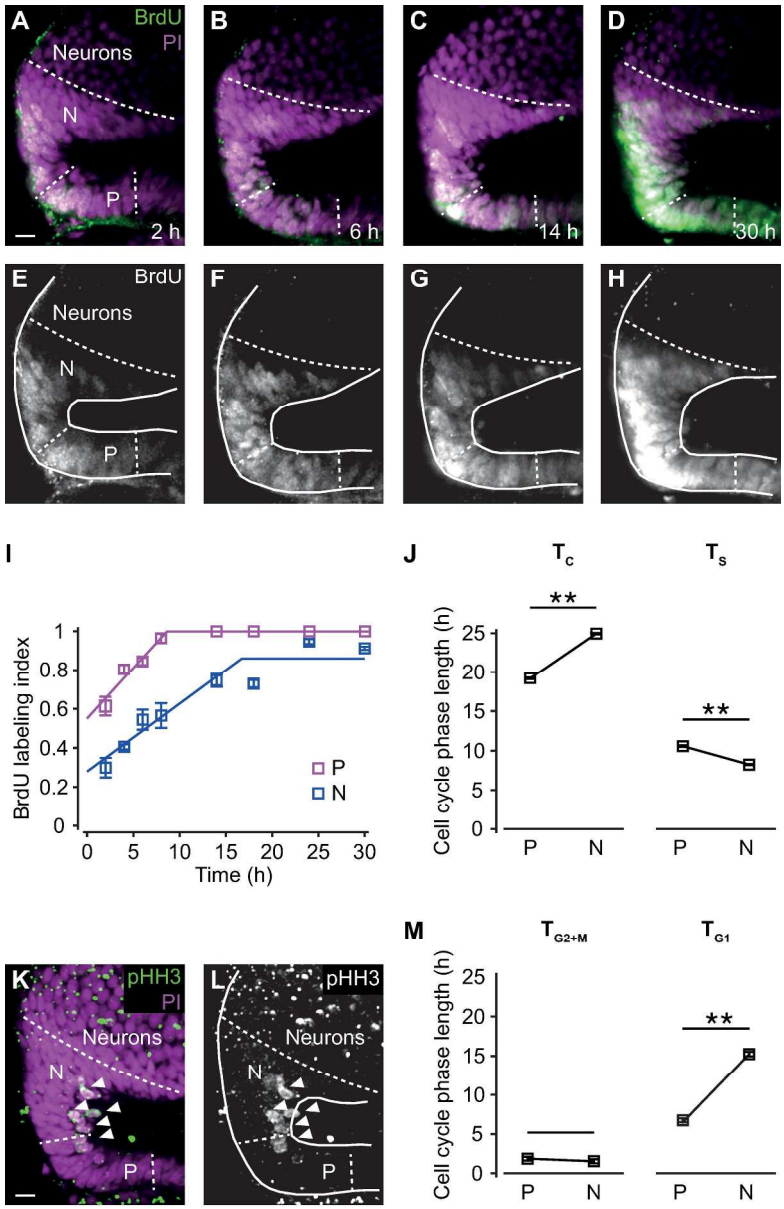

Figure 7 The length of the cell cycle, S phase and G1 phase differ between proliferative and neurogenic regions of the optic tectum. (A-D) The optic tectum stained for BrdU (green) and cell nuclei (magenta) after 2 hours (A), 6 hours (B), 14 hours (C) and 30 hours (D) of incubation with BrdU. P, proliferative region. N, neurogenic region. Scale bar represents 10 µm. (E H) BrdU immunoreactivity from the images shown in (A-D). (I) Quantification of the fraction of BrdU+ cells over time in the proliferative and neurogenic regions. n = 22 animals. (J) Length of cell cycle (left) and length of S phase (right) in proliferative and neurogenic regions. (K) The optic tectum stained for phospho-histone H3 (green) and cell nuclei (magenta). Phospho-histone H3+ cells (arrowheads) exhibited clear somatic labeling and reside near the ventricular wall. In contrast, staining in the neuronal region is not associated with cell somata. n = 6 animals. Scale bar represents 10 µm. (L) Phospho-histone H3 immunoreactivity from the image shown in (K). (M) Combined length of G2 phase and M phase (left) and length of G1 phase (right) in proliferative and neurogenic regions. All population data are displayed as mean ± sem. **, $p < 0.01$ in unpaired t-test with Welch's correction.
200x310mm (300 x 300 DPI)